

CHARACTERIZATION OF CRYO-ROLLED LOW CARBON STEEL USING FERRITE-MARTENSITE STARTING MICROSTRUCTURE

S.A.Zakaria ^a, M. S. Ahmad ^a, A.S.Anasyida ^{a,*}, H.Zuhailawati ^a, B.K. Dhindaw ^b, T.E.Abioye ^c

^a School of Materials & Mineral Resources Engineering, Universiti Sains Malaysia, Penang, Malaysia

^b Indian Institute of Technology Kharagpur, India

^c Industrial and Production Engineering Department, School of Engineering and Engineering Technology, Federal University of Technology Akure, Akure, Nigeria

(Received 07 March 2023, Accepted 14 December 2023)

Abstract

Cryo-rolling, a technique of severe plastic deformation (SPD) performed at cryogenic temperatures, has proven to be a promising technique for improving the microstructure and mechanical properties of low-carbon steels. Low carbon steel with a two-phase ferrite-martensite starting microstructure was subjected to cryogenic rolling at liquid nitrogen temperature to produce sheets with different deformation rates: 50%, 70%, and 90%. The microstructure, mechanical properties, and corrosion resistance were investigated. The results show that cryo-rolling effectively refines the microstructure and leads to a higher dislocation density and smaller grain size as the deformation rate increases. The cryo-rolled sample deformed at 90% has the highest grain aspect ratio (35.5), the smallest crystallite size (13.70 nm), the highest lattice strain (74.6×10^{-3}), and the highest dislocation density compared to the samples deformed at 50% and 70%. This refined microstructure significantly improves the mechanical properties, with the cryo-rolled sample deformed at 90% exhibiting the highest hardness (152 HV), tensile strength (1020 MPa), and yield strength (950 MPa), corresponding to an increase of 175.6%, 344.0%, and 466.5%, respectively. In addition, cryo-rolling at 90% showed a decrease in corrosion resistance, with the lowest corrosion rate observed at 90% deformation (5.97 mm/year).

Keywords: Low carbon steel; Dual-phase structure; Ferrite-martensite; Cryogenic rolling; Mechanical properties; Corrosion resistance

1. Introduction

Severe plastic deformation (SPD) in metal processing has become increasingly important in materials research, as it allows for grain refinement to sub-micrometer (100 nm - 1 μ m) or even nanometer (100 nm) sizes in conventional bulk solids [1, 2, 3]. The grain size of polycrystalline materials affects their fundamental characteristics, so SPD can produce materials with unusual and attractive properties, such as extraordinary improvements in mechanical properties, and with minimal processing defects, such as porosity and impurities [4]. Various SPD processes can be used to develop ultrafine-grained (UFG) samples of different shapes and sizes. For example, equal channel angular pressing (ECAP) develops UFG samples in the form of rods and bars, while friction stir processing and cryo-rolling can produce UFG plates or sheets. Asymmetric rolling, cryo-rolling, and accumulative roll bonding are suitable techniques for forming UFG sheets [5]. Cryo-rolling, in particular, is a well-established technique for

producing ultrafine-grained sheets of pure metals and alloys from their bulk counterparts by deforming them at cryogenic temperatures with much less strain than other SPD processes performed at ambient or high temperatures [6].

The initial microstructure of steel are ferrite+pearlite and ferrite+martensite. Ferrite-martensite has been identified as the best initial microstructure to improve the mechanical properties of ultrafine-grained steel. Currently, rolling and annealing are used to refine the ferrite-martensite starting microstructure [7]. Yaghoobi et al. [8] investigated the effect of holding time at a constant intercritical temperature on the microstructure and mechanical properties of a ferrite-martensite dual-phase (DP) structure. Plain carbon steel with 0.16% carbon was subjected to heat treatment at 830 °C for 1, 5, and 15 minutes, followed by quenching. They found that the hardness and strength were higher (354.1 HV and 1172.5 MPa, respectively) than those of the as-received material, but the total elongation was lower (13.5%). Similarly, Balbi et al. [9]

Corresponding author: anasyida@usm.my

<https://doi.org/10.2298/JMMB230307038Z>



successfully produced an ultrafine ferrite-martensite microstructure of low carbon steel (0.09% carbon) by annealing at intermediate temperatures. The ultimate and yield strength were 670 MPa and 400 MPa, respectively. Furthermore, Molaei and Ekrami [10] reported that intercritical annealing resulted in a fibrous morphology, ultimate strength (UTS) of 812 MPa, yield strength (YS) of 702 MPa, and total elongation (TE) of 15.1% in low carbon steel (0.23% carbon).

In addition, Park et al. [11] investigated the process of cold rolling combined with intercritical annealing of low carbon steel (AISI 1015) to produce a high-strength DP structure. The sample was reduced by 60% and intercritical annealed at 750°C for 5 minutes. They observed that the martensite grains formed a chain-like network structure around the ferrite grain, and they reported that the UTS, YS, and TE of the DP structure were 947 MPa, 458 MPa, and 12.5%, respectively. Jing et al. [12] produced an ultrafine grain steel sheet by a combination process of quenching, aging, heavy cold rolling, and annealing. They reported that work hardening of dual-phase steel containing ferrite-martensite phase exhibits optimum mechanical properties in terms of strength and ductility. In contrast, Yuan et al. [13] focused on refining the structure of low carbon steel with a ferrite-martensite microstructure using cryo-rolling and subsequent annealing. The UTS increased to 970 MPa and the grain size reduced to 133 nm.

In addition to the mechanical properties discussed above, low carbon steel processed by cryo-rolling exhibits unique corrosion behavior. While cryo-rolling effectively refines the microstructure and enhances the mechanical properties of steel, its effect on corrosion resistance is more complex. The corrosion resistance of the material deteriorates during the Severe Plastic Deformation (SPD) process, primarily due to the high defect densities induced in the material [14]. The corrosion is particularly associated with the structural inhomogeneity resulting from the intense plastic deformation that induces lattice defects. These structural irregularities give rise to local variations in surface potential and higher reactivity in the grain boundaries [15]. Grain boundaries serve as preferential sites for corrosion attacks due to their imperfect atomic arrangement, leading to rise in local energy, increase volumes, and stresses. The increases of volume fraction of grain boundaries and dislocation density in cryo-rolled sample accelerates the corrosion rate. According to the thermodynamic principles of electrochemistry, ultrafine-grained (UFG) materials exhibit lower dissolution potential and, consequently a higher

dissolution in aggressive environments compared to their coarse-grained. This is attributed to the high density of grain boundaries and higher internal energy [16]. Shit and Ningshen [17] investigated the corrosion behavior of cryo-rolled low carbon steel in nitric acid solution and found that cryo-rolling at 90% deformation resulted in a decrease in corrosion resistance compared to the as-received material. This result aligns with Singh and Pandey [18], who investigated the effect of cryo-rolling on corrosion resistance of low carbon steel and found that cryo-rolling initially enhanced corrosion resistance due to refining of the microstructure. However, at higher deformation rates, a decrease in corrosion resistance was observed. At a deformation rate of 95%, the cryo-rolled low carbon steel showed a pronounced decrease in corrosion resistance, with a substantial 15% reduction compared to the unrolled steel. This decrease in corrosion resistance is attributed to the formation of finer grains in the microstructure of the cryo-rolled steel at higher deformation rates. These fine grains provide more nucleation sites for corrosion pits, leading to an increased corrosion rate [19].

There are few studies focusing on the cryo-rolling of plain carbon steels to fabricate ultrafine grains by comparing the microstructure and mechanical properties. However, the impact of rolling reduction during cryo-rolling on the grain size, lattice strain, mechanical properties, and corrosion behavior of low carbon steel has not been thoroughly explored. Hence, this study aims to refine the grains of low-carbon steels with ferrite+martensite structure by cryo-rolling at various thickness reductions and investigate the microstructure, lattice strain, mechanical properties, and corrosion behavior. The results obtained in this study can be utilized as a reference for producing ultrafine-grained low-carbon steel with the desired properties.

2. Materials and methods

2.1. Material

Table 1 shows the chemical composition (in wt.%) of low carbon steel material. The material is procured from Terra Techno Engineering (TTE), Selangor, Malaysia. The alloy was received in plate size of 600 x 100 x 5 mm. The chemical composition (in wt.%) of low carbon steel material used is listed in Table 1.

2.2. Methods

The plates were cut into dimensions of 100 x 10 x 5 mm using hydraulic cutting machine. The inter critical temperatures AC1 (746°C) and AC3 (865°C)

Table 1. Chemical composition (wt.%) of low carbon steel

Fe	C	Si	Mn	P	Cr	Ni	Cu	Al
99.53	0.06	0.03	0.14	0.01	0.03	0.02	0.09	0.03



were calculated, following ASTM A-1033-04 [20] using equations (1) and (2) [21]:

$$AC1(^{\circ}C) = 751 - 16.3(C) - 27.5(Mn) - 5.5(Cu) - 5.9(Ni) + 34.9(Si) + 12.7(Cr) + 3.4(Mo) \quad (1)$$

$$AC3(^{\circ}C) = 881 - 206(C) - 15(Mn) - 26.5(Cu) - 20.1(Ni) - 0.7(Cr) + 53.1(Si) + 41.7(V) \quad (2)$$

In order to create the two-phase structure, the low carbon steel was first heated to 950 °C for 30 minutes and then quickly quenched in ice water. The sample was then heated to an inter-critical temperature (830 °C), held for 3 minutes and quenched in ice water and referred to as quenched sample. Following heat treatment, the specimens were subjected to cryo-rolling using a custom two-roll mill machine. The cryo-rolling process included dipping the sample in liquid nitrogen for 15 minutes and then followed by rolling. In between the rolling passes, the sample was dipped in liquid N₂ to maintain the cryogenic temperature. Three reduction levels (50%, 70%, and 90%) were chosen to investigate the effect of cryo-rolling on grain refinement, mechanical properties, and corrosion behavior. The number of rolling passes for each reduction level was determined to achieve the desired thickness reduction while minimizing the risk of cracking as follows; 50% reduction – 50 passes, 70% reduction – 70 passes, and 90% reduction – 120 passes. Throughout the cryo-rolling process, a constant rolling speed of 1 m/s was maintained, and the temperature of the rolling mill was –196 °C.

Microstructure and phase present in the sample were investigated by optical microscope (OM) and X-ray Diffractometer (XRD). For OM observation, the sample was initially ground by SiC paper of different grit sizes and finished by polishing. The microstructure was revealed by etching in the 2% of Nital solution and observed using OM (model Meiji equipped with image analyzer i-Solution DT software). X-ray diffractometer D8 Bruker Advanced X-ray was used to measure the crystallite size, lattice strain and dislocation density of the sample for 2 θ ranging from 20° to 90°. The XRD analysis was conducted according to ASTM E337-18 [22]. The crystallite size (τ) (equation 3), lattice strain (η) (equation 4), and dislocation density (ρ) (equation 5) of the samples were determined using the Scherrer equation which is expressed as [23]:

$$\tau = k\lambda / \beta(\cos \theta) \quad (3)$$

where k is a constant known as the Scherrer constant.

The lattice strain (η) of the sample can be calculated from the FWHM of the diffraction peak using the following equation:

$$\eta = \beta / (4 \tan \theta) \quad (4)$$

The dislocation density (ρ) of the sample can be estimated from the crystallite size and lattice strain using the following equation:

$$\rho = (3\sqrt{2\pi}) / Db[(\eta^2)^{(1/2)}] \quad (5)$$

where D is the grain size, b is the Burger's vector, and η is the lattice strain.

Mechanical properties of the sample were analyzed through hardness and tensile testing. The Vickers hardness testing was conducted at room temperature with a load of 300 gf and a dwell time of 10 seconds, following ASTM E92-18 [24] and 10 readings were taken from each sample at different location. Average value of these reading was used to plot the hardness data. For the tensile test, the specimens were machined into the ASTM E8M [25] sub-sized specimen with a gauge length of 50 mm. Uniaxial tensile tests were carried out at crosshead speed of 1 mm/min using Instron Universal Testing. For tensile testing, five samples were tested in each processing condition and average of five test results were used to plot stress-strain curve. Fractured surface after tensile test was analyzed through Carl Zeiss SUPRA 35V Field Emission Scanning Electron Microscopy (FESEM) using secondary electron (SE) and backscattered (BSE) modes.

The corrosion test was conducted using a three-electrode configuration in a 3.5 wt.% NaCl solution at room temperature, with a PGSTAT 101 Autolab potentiostat. A saturated calomel electrode (SCE) and platinum electrode served as the reference and counter electrodes, respectively. The polarization potentials ranged from -1.00 to 1.00 V, with a slow scanning rate of 0.01 V/s, and the Tafel extrapolation method was used to determine the corrosion properties of the tested samples. The corrosion test was conducted according to ASTM G5-15 [26].

3. Results & discussion

3.1. Microstructural analysis

The optical micrographs of as-received, quenched and cryo-rolled samples at different thickness reductions are shown in Figure 1. Microstructure of as-received material consisted of ferrite and pearlite phases that had regular shapes and an average size of 11.42 μm (Figure 1a) while as-quenched sample consisted of ferrite-martensite phases that had irregular shape with an average grain size of 14.24 μm (Figure 1b).

In comparison, the sample with a 50% thickness reduction had an elongated grain but a wider grain width than the sample with a 70% thickness



reduction. The sample with a 70% thickness reduction had a greater degree of strain, as indicated by the appearance of small grains at the grain boundaries in Figure 1d. When the thickness reduction was lowered to 90%, the existing grain boundaries were not easily discernible and the grain became fragmented at the grain boundaries, leading to elongated grains in the rolling direction and the development of a fibrous structure. Cryo-rolling induced high strain that caused the accumulated dislocation density to transform the grains into new, smaller grains, initiating the nucleation of small grains.

The grain aspect ratio of the samples was measured and tabulated in Table 2. The grain aspect ratio was estimated based on the ratio of grain's length, l to the ratio of grain's width, w . The value represents the distortion of grains as the deformation occurred [27, 28]. From Table 2, it can be observed that the percentage reduction affected the value of grain aspect ratio. The grain aspect ratio increased as the

percentage of thickness reduction increased. The highest grain aspect ratio calculated was 35.5 and was attained at 90% of thickness reduction. Higher grain aspect ratio indicated the sample had severe deformed grain and the grain size became thinner. The sample with 50% of thickness reduction had the lowest grain aspect ratio (7.3) while, the grain aspect ratio of as-received material and quenched sample were 1.6 and 3.3. This showed that the cryo-rolled sample at 90% thickness reduction had a significant reduction in grain size. Besides that, the difference in grain aspect ratio demonstrated that different thickness reduction with different strain applied during cryo-rolling process would result in difference grain distortion and directional grain orientation along the rolling direction.

3.2. X-ray diffraction analysis

Figure 2 shows the phase analysis of as received,

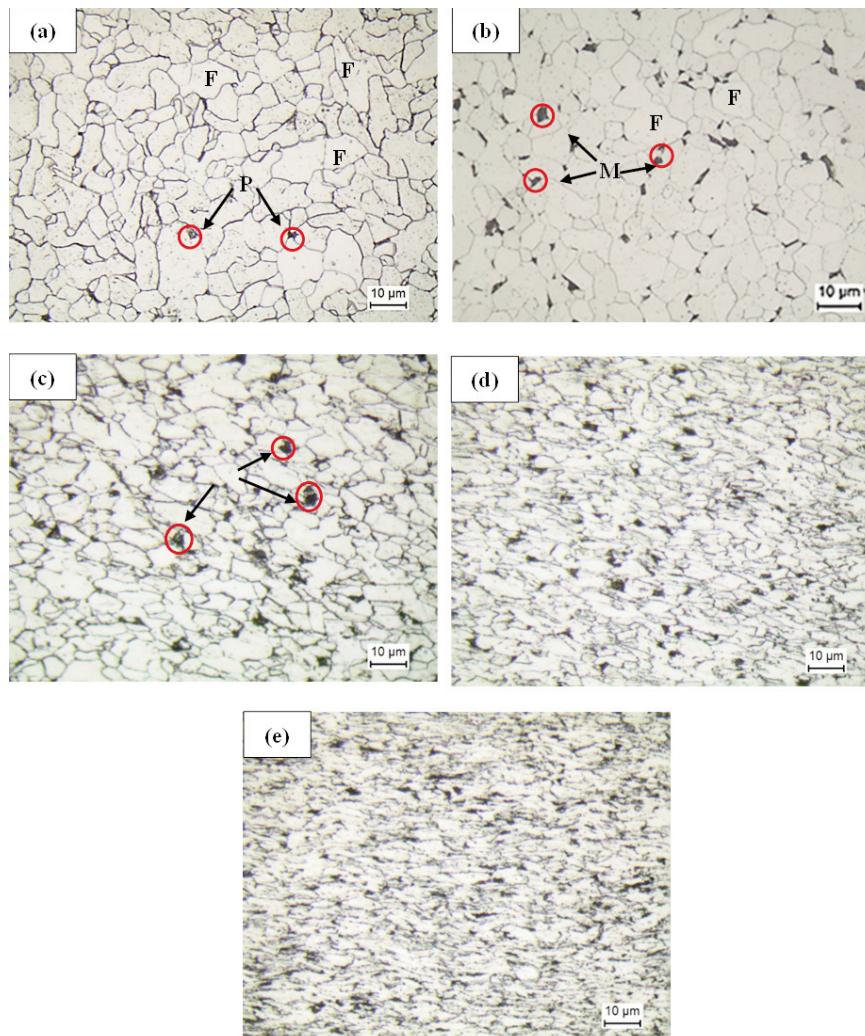
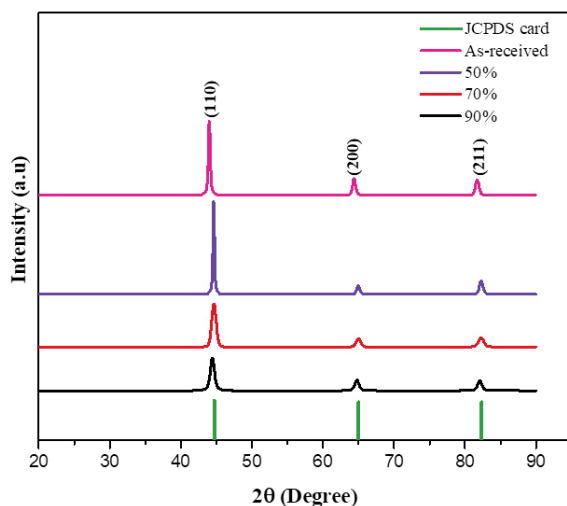


Figure 1. Microstructure of cryorolled low carbon steel at various thickness reductions (a) as received material (ferrite+pearlite), (b) as-quenched (ferrite+martensite), (c) 50%, (d) 70%, and (e) 90%

Table 2. Grain aspect ratio of as-received and cryorolled low carbon steel at various thickness reduction

Sample condition	Grain aspect ratio
As-received	1.58 ± 3.67
As-quenched	3.25 ± 2.14
50% reduction	7.29 ± 2.53
70% reduction	15.83 ± 2.27
90% reduction	35.47 ± 5.15

and cryo-rolled samples with JCPDS card no of 04-014-0360. The full width at half maximum intensity values were utilized to measure peak broadening and intensity reduction, as outlined in Table 3. A contrasting trend in crystallite size and lattice strain was observed between the as-received material and cryo-rolled samples. The cryo-rolled sample with a 50% thickness reduction had a crystallite size of 23.04 nm and a lattice strain of 33.52×10^{-3} . As the thickness reduction was reduced to 70%, the crystallite size decreased to 15.09 nm, and the lattice strain increased to 40.72×10^{-3} . The crystallite size decreased to 13.70 nm, and the lattice strain increased to 74.6×10^{-3} when the thickness reduction was lowered by 90%. In comparison to the as-received material, both the crystallite size and lattice strain were reduced by 58.9% and increased by 425.5%, respectively, following a 90% reduction. The strain imposed during cryo-rolling could have induced distortion in the grains, resulting in a smaller crystallite size and higher lattice strain [29]. The decrease in crystallite size could also be attributed to the accumulation of dislocation density throughout the cryo-rolling process [30]. Additionally, the highest dislocation density value (85.29×10^{11}) was obtained after a 90% reduction. During the early stages of deformation, structural refinement and a rise in dislocation density

**Figure 2.** X-ray diffraction of as-received, and cryorolled low carbon steel at various thickness reductions

occurred rapidly, while subsequent cryo-rolling resulted in an increase in dislocation density.

3.3. Hardness

Figure 3 illustrates the Vickers microhardness values obtained with a 3 kg load for various thickness reductions. The hardness value increased with increasing thickness reduction, reaching a maximum value of 429.4 HV in the cryo-rolled sample with a 90% reduction. This represents a 175.6% improvement compared to the as received (155.8 HV) and as-quenched sample (220.3 HV). The cryo-rolled sample with a 50% thickness reduction exhibited the lowest hardness value of 267.9 HV, while the hardness increased to 305.9 HV when the thickness reduction was increased to 70%. This increase was attributed to the high amount of strain applied to the sample. Comparing the cold rolled and cryo-rolled sample for thickness reduction of 90%, a notable improvement of 43.8% was observed in the cryo-rolled sample.

3.4. Tensile Properties

Figure 4 depicts the relationship between tensile and yield strength of cryo-rolled low carbon steel at different thickness reductions. The results show a gradual increase in strength and a decrease in elongation percentage with increasing thickness reduction. The sample with 90% thickness reduction achieved the highest tensile and yield strength of 1537 MPa and 1495 MPa, respectively. This represents a significant improvement of 344.0% and 466.5% compared to the as-received material, which can be attributed to the high accumulation of dislocation density that acts as an effective barrier to dislocation movement during deformation, as indicated in Table 4. As the thickness reduction increased, the ductility of the cryo-rolled sample decreased. The elongation of

Table 3. Full width at half maximum intensity, crystallite size, lattice strain and dislocation density of as-received and cryo-rolled low carbon steel at various thickness reduction

Sample condition	Full width at half maximum intensity (radians)	Crystallite size (nm)	Lattice strain (10^{-3})	Dislocation density (10^{11} m^{-2})
As-received	0.0067	33.3107	14.2026	11.2263
50% reduction	0.0073	23.0371	33.516	64.4225
70% reduction	0.0122	15.0922	40.7227	71.0456
90% reduction	0.0133	13.6983	76.621	85.2876

the as-received material was 44.03%, which decreased to 13.99%, 7.99%, and 6.35% after cryo-rolling at 50%, 70%, and 90% thickness reduction, respectively. The high density of dislocation in the material created more obstacles for dislocation movement during deformation, leading to reduced elongation. Sample that was cold rolled at 90% showed a low strength compared to cryo-rolled sample at 90%. This indicated that cryo-rolling had a great impact on the changes of microstructure that lead to the increase in strength.

The stress-strain engineering curve of cryo-rolled low carbon steel at different thickness reductions is shown in Figure 5. It is evident from the plot that the cryo-rolled steels exhibit an increase in ultimate tensile strength (UTS) because of strain hardening. The strain hardening exponent of the cryo-rolled steels also increased with an increase in thickness reduction. The elevated level of dislocation in steels with higher thickness reduction required greater force to deform the sample, resulting in a higher strain

hardening exponent value. A material with a higher strain hardening coefficient possessed greater formability compared to materials with a lower value. This is because materials with higher values of strain hardening coefficient demonstrate greater resistance to necking, allowing for further stretching before necking initiates [31].

3.5. Fracture morphology

The fracture surface of cryo-rolled low carbon steel at various thickness reductions was analyzed using FESEM, and the results are presented in Figure 6. The figure illustrates that all the fracture specimens of cryo-rolled steels exhibited a mixed fracture mode, consisting of both ductile and brittle features. The surface contained well-developed dimples distributed over the entire surface, which represented the ductile mode, and some facets that represented the brittle mode. However, the number of small dimples and

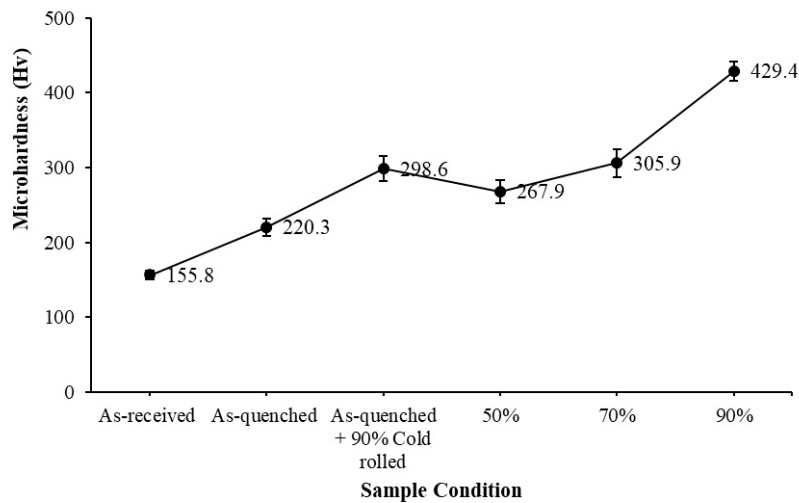


Figure 3. Microhardness of as-received, as-quenched and cryo-rolled low carbon steel at various thickness reduction

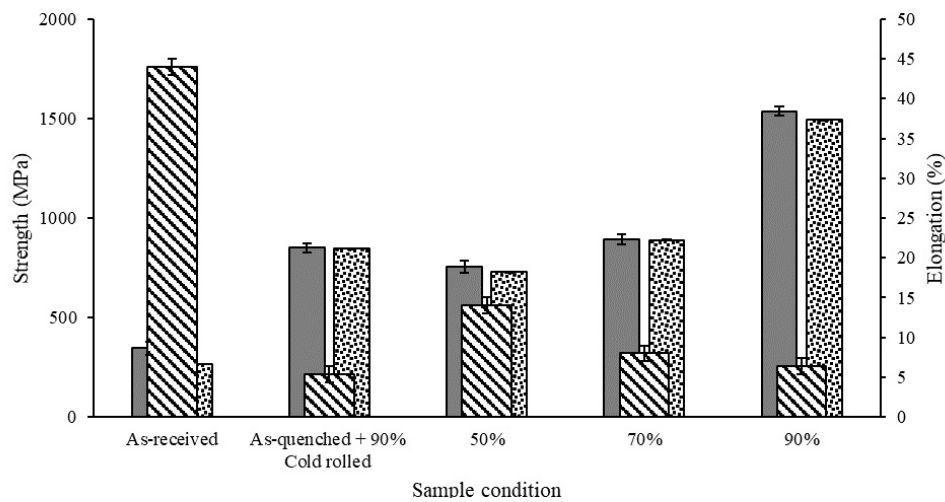


Figure 4. Tensile properties and elongation of as-received and cryo-rolled low carbon steel at various thickness reduction

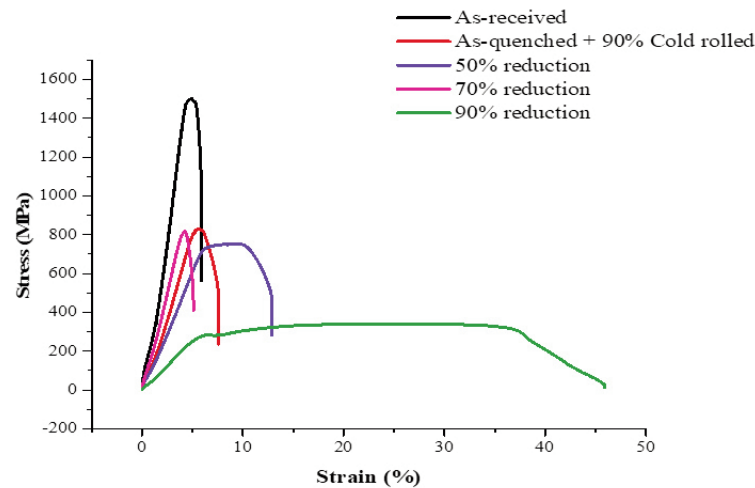


Figure 5. Stress-strain engineering curve of as-received, as-quenched + 90% cold rolled, and cryo-rolled low carbon steel at various thickness reduction

Table 4. Strain hardening coefficient of cryo-rolled low carbon steel at various thickness reduction

Percentage reduction	As-received	As-quenched + 90% cold rolled	50%	70%	90%
Strain hardening coefficient (n)	0.11	0.22	0.13	0.25	0.56

their size increased with decreasing thickness reduction. In Figure 6(a), the fracture surface of the as-received material exhibited a typical ductile fracture morphology, with larger dimple size and a small amount of facets. In contrast, the number of large and deep dimples decreased with decreasing thickness reduction (Figure 6b-d). This phenomenon suggested that the fracture morphology of low carbon steel changed from typical ductile to a mixture of ductile-brittle fracture after cryo-rolling.

Figure 6(b) shows the fracture surface of cryo-rolled low carbon steel at 50% thickness reduction, exhibiting deep and large dimples, with an average size of 4.3 μm . In contrast, the fracture surface of the sample at 70% reduction (Figure 6c) displayed shallower and smaller dimples, with an average size of 3.31 μm . Further reduction of thickness to 90% resulted in an even smaller average dimple size of 2.47 μm and shallower dimple depth. This phenomenon can be explained by the effect of grain refinement that occurred during plastic deformation of the specimens. Cryo-rolled sample at 50% reduction had coarser grain than the sample at 70% and 90% reduction, resulting in wider dimples, which was caused by the fracture of large martensite particles. In contrast, the finer grain size of the sample cryo-rolled at 90% reduction led to the ferrite-martensite interface becoming the main location for the nucleation of voids, and the high nucleation density of voids prevented excessive growth of voids. As a result, the coalescence of adjacent voids created a fracture surface containing small-sized dimples, as shown in Figure 6(d). The high density of coalescence nucleated voids served as a significant brittle fracture

mechanism in ultra-fine grain low carbon steel [32].

3.6. Corrosion analysis

3.6.1. Polarization

The corrosion performance of cryo-rolled low carbon steel with different thickness reductions (50%, 70%, and 90%) was investigated using potentiodynamic polarization testing, and the corresponding polarization curve is presented in Figure 7. The corrosion potential (E_{corr}), corrosion current density (i_{corr}), and corrosion rate of the as-received material and cryo-rolled low carbon steels were recorded and are listed in Table 5. The results show that i_{corr} and corrosion rate increased with grain refinement. The rise in i_{corr} could be attributed to the effect of grain boundaries, as their high density promotes surface reactivity through increased electron activity and diffusion [33]. It is observed that i_{corr} gradually increased after 50% deformation and then accelerated significantly at 90% deformation. The corrosion rate of cryo-rolled steel decreased to 2.29 mm/yr, 3.38 mm/yr, and 5.97 mm/yr at 50%, 70%, and 90% reduction, respectively, whereas the as-received material exhibited the lowest corrosion rate of 1.12 mm/yr.

The corrosion resistance of the material decreased during severe plastic deformation (SPD) due to the high density of defects induced in the structure. The structural inhomogeneities led to higher grain boundary reactivity and a local potential difference on the surface, making the grain boundaries a preferred site for corrosion attacks [15]. This is exacerbated by the increasing dislocation density and volume fraction of

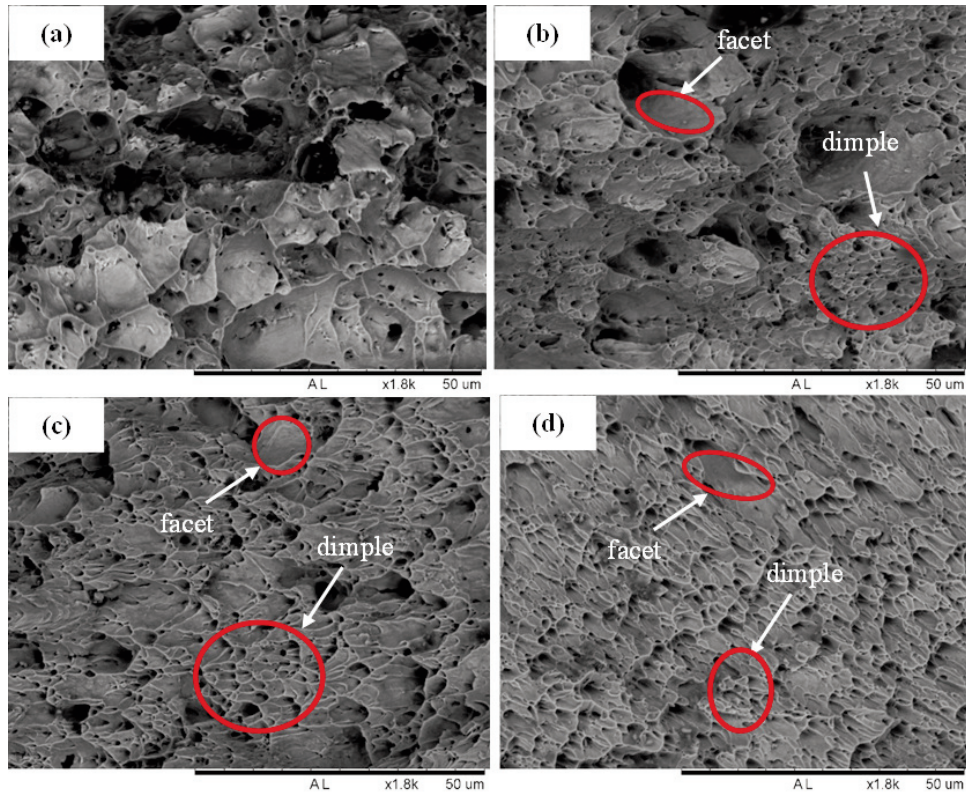


Figure 6. Fracture morphology of as-received and cryorolled low carbon steel at various thickness reduction, (a) as-received, (b) 50%, (c) 70% and (d) 90%

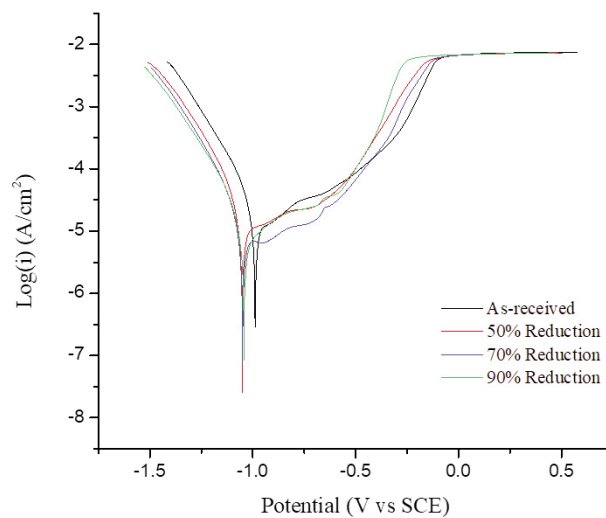


Figure 7. Potentiodynamic polarization curve of as-received and cryo-rolled low carbon steel at various thickness reduction

Table 5. Corrosion potential (E_{corr}), current density (i_{corr}), and corrosion rate of as-received and cryo-rolled low carbon steel at various thickness reduction

Sample condition	E_{corr} (V)	i_{corr} (A/cm ²)	Corrosion rate (mm/year)
As-received	-0.9909	9.6e-05	1.13
50% reduction	-1.0529	0.000197	2.29
70% reduction	-1.0521	0.00029	3.38
90% reduction	-1.0462	0.000512	5.97

boundaries during the cryo-rolling process, leading to a faster corrosion rate. Additionally, as the thickness was further reduced, the dislocation density increased, making corrosion initiation more favorable in the deformation region. The interface area between the dislocation networks may also contribute to the increased activity of such sites to metal dissolution, resulting in a higher corrosion rate.

3.6.2. Immersion test

Table 6 presents the weight loss results for both as-received and cryo-rolled low-carbon steel samples with varying thickness reductions after immersion in 300 mL of 3.5% NaCl solution for seven days. The corresponding SEM images of the corroded surfaces are presented in Figure 8. A uniform corrosion

Table 6. Initial weight, final weight, weight loss and weight loss in percent of as-received and cryo-rolled low carbon steel at various thickness reduction

Sample condition	Initial weight (g)	Final weight (g)	Weight loss (g)	Weight loss (%)	Corrosion rate (mm/y)
As-received	3.2766	3.274	0.0027	0.08	5.32
50% reduction	1.7881	1.7858	0.0023	0.13	8.65
70% reduction	1.2545	1.2521	0.0024	0.19	12.64
90% reduction	0.6996	0.697	0.0026	0.37	24.61

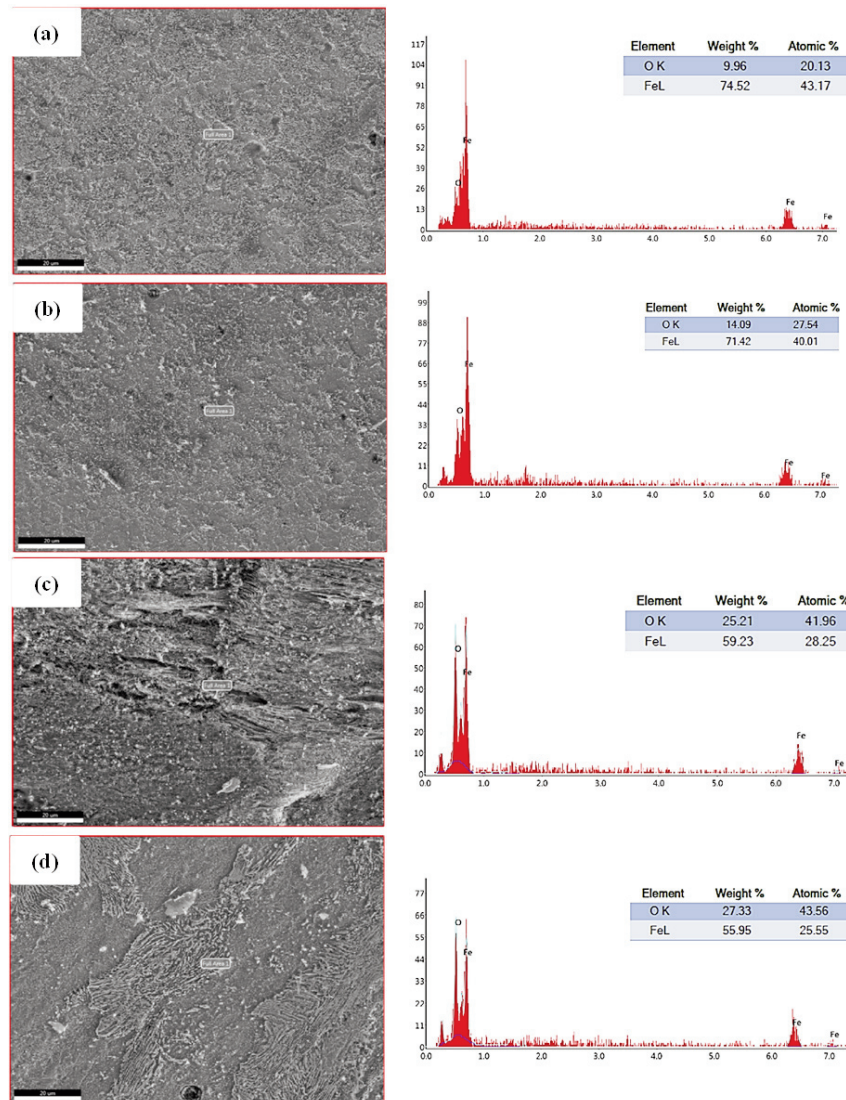


Figure 8. Surface morphology of (a) as-received and cryo-rolled (b) 50% reduction (c) 70% reduction (d) 90% reduction samples after immersion test

products were observed on all the samples. The sample of cryo-rolled had more amount of iron oxide compared to as-received as indicated in the EDX analysis. The corrosion products formed on the sample surface was due to the diffusion of dissolved oxygen at the interface between steel and solution. The outer layer consisted of γ -FeOOH gradually transformed to porous α -FeOOH, which had limited protection to the steel. However, in the inner layer that consisted of γ -FeOOH it was transformed into Fe_3O_4 and Fe_2O_3 to form a more stable iron oxide [3]. The findings from the immersion test correlate with the potentiodynamic polarization results based on corrosion rate readings. The weight loss percentage of cryo-rolled low carbon steel increased as the thickness reduction increased, suggesting that cryo-rolling caused a change in microstructure, causing in increased internal strain and residual stress within the grain, as supported by reference [34]. Cryo-rolling generated internal stress in the sample and reduced the mobility of dislocation, thus affecting the corrosion behavior of the cryo-rolled sample compared to the as-received material. Among the cryo-rolled samples, the one with 90% reduction recorded the highest corrosion rate of 24.61 mm/year, while those with 50% and 70% reduction had corrosion rates of 12.64 and 8.65 mm/year, respectively. This was because all cryo-rolled samples experienced different levels of strain hardening, which induced a varying degree of dislocation density in the grain boundary. In contrast, the as-received material had the lowest corrosion rate of 5.32 mm/year.

4. Conclusion

The formation of fine sub-grains within the structure resulted in a higher increase in grain aspect ratio (117.1% to 386.6%) for samples with 70% to 90% reduction compared to those with 50% reduction. The same pattern was observed for dislocation density, lattice strain, and mechanical properties. The sample with 90% reduction had the highest grain aspect ratio (35.47), the highest dislocation density ($85.28 \times 10^{11} \text{ m}^{-2}$), and the smallest crystallite size (13.7 nm).

Cryo-rolling at 90% reduction resulted in higher microhardness and tensile strength with increase of 157.5% and 343.9%, respectively, compared to the as-received low carbon steel. Fracture morphology of the cryo-rolled sample showed many facets and small-sized dimples, indicating a transformation from a typical ductile behavior (as-received material) to a mixture of ductile-brittle fractures.

The corrosion rate of cryo-rolled samples was higher compared to the as-received material, with the sample deformed at 90% reduction exhibiting the highest corrosion rate (5.97 mm/yr). The corrosion

resistance decreased due to the increment of dislocation, located defect, and stress along with strain hardening.

Acknowledgment

The authors would like to thank to MYTRIBOS for providing the fund for this study under MYTRIBOS Industrial Grant, grant no. 304 /PBAHAN /6050471 /M171.

Author Contributions

S.A.Zakaria - Draft manuscript preparation, M.S.Ahmad - Experimental work and data collection, A.S.Anasyida - design and supervision, H.Zuhailawati - analysis and interpretation of results, B.K. Dhindaw- critical review, T.E.Abioye - editing manuscript. All authors reviewed the results and approved the final version of the manuscript.

Conflict of Interest

The authors declare that they have no known competing financial interests or personal relationships that could have appeared to influence the work reported in this paper.

Compliance with Ethical Standards

The work is compliant with ethical standard.

References

- [1] R.B.Figueiredo, T.G.Langdon, Fabricating ultrafine-grained materials through the application of severe plastic deformation: a review of developments in Brazil, *Journal Material Research Technology*, 1 (1) (2012) 55-62. [https://doi.org/10.1016/S2238-7854\(12\)70010-8](https://doi.org/10.1016/S2238-7854(12)70010-8).
- [2] K.Changela, H.Krishnaswamy, R.K.Digavalli, Development of combined groove pressing and rolling to produce ultra-fine grained Al alloys and comparison with cryorolling, *Material Science and Engineering A*, 760 (2019) 7-18. <http://dx.doi.org/10.1007/s11661-019-05532-2>.
- [3] S.A.Zakaria, M.P.Lew, A.S.Anasyida, M.N.Idris, H.Zuhailawati, A.Ismail, Mechanical and corrosion properties of low-carbon steel processed by cryorolling: Effect of different initial microstructures, *Arab Journal Science Engineering*, 46(8) (2021) 7815-7825. <https://doi.org/10.1007/s13369-021-05507-9>.
- [4] D.Fuloria, S.Goel, R.Jayaganthan, D.Srivastava, G.K.Dey, N.Saibaba, Mechanical properties and microstructural evolution of ultrafine grained zicaloy-4 processed through multiaxial forging at cryogenic temperature, *Transaction of Nonferrous Metal Society of China*, 25 (2015) 2221-2229. [https://doi.org/10.1016/S1003-6326\(15\)63835-3](https://doi.org/10.1016/S1003-6326(15)63835-3).
- [5] Y.Huang, T.G.Langdon, Advances in Ultrafine-grained Materials, *Materials Today*, 16(3) (2013) 85-93.



- <https://doi.org/10.1016/j.mattod.2013.03.004>.
- [6] A.Dhal, S.K.Panigrahi, M.S.Shunmugam, Strengthening and Joining by Plastic Deformation, Springer, Singapore, 2019, p.246.
- [7] Q.Yuan, G.Xu, S.Liu, M.Liu, H.Hu, G.Li, Effect of rolling reduction on microstructure and mechanical property of ultrafine grain low-carbon steel processed by cryorolling martensite, *Metals*, 8(7) (2018) 1-14. <https://doi.org/10.3390/met8070518>.
- [8] F.Yaghoobi, R.Jamaati, H.J.Aval, A new 1.2 GPa-strength plain low carbon steel with high ductility obtained by SRDR of martensite and intercritical annealing, *Material Science and Engineering A*, 788 (2020) 139584. <https://doi.org/10.1016/j.msea.2020.139584>.
- [9] M.Balbi, I.Alvarez-armas, A.Armaz, Effect of holding time at an intercritical temperature on the microstructure and tensile properties of a ferrite-martensite dual phase steel, *Materials Science and Engineering A*, 733 (2018) 1-8. <https://doi.org/10.1016/j.msea.2018.07.029>.
- [10] M.J.Molaei, A.Ekrami, The effect of dynamic strain aging on fatigue properties of dual phase steels with different martensite morphology, *Material Science and Engineering A*, 527 (2009) 235-238. <https://doi.org/10.1016/j.msea.2009.08.005>.
- [11] K.Park, M.Nishiyama, N.Nakada, T.Tsuchiyama, S.Takaki, Effect of the martensite distribution on the strain hardening and ductile fracture behaviors in dual phase steel, *Materials Science and Engineering A*, 204 (2014) 135-141. <https://doi.org/10.1016/j.msea.2014.02.058>.
- [12] T.Y. Jing, G. Xu, W.C. Liang, Q.Yuan, Effect of annealing on the microstructure and mechanical properties of a low-carbon steel, *Metallography Microstructure Analysis*, 6 (2017) 233-239. <https://doi.org/10.1007/s13632-017-0350-0>.
- [13] Q.Yuan, G.Xu, M.Liu, S.Liu, H.J. Hu, Evaluation of mechanical properties and microstructures of ultrafine grain low-carbon steel processed by cryorolling and annealing, *Transactions of the Indian Institute of Metals*, 72(3) (2019) 741-749. <https://doi.org/10.1007/s12666-018-1526-2>.
- [14] N.Rangaraju, T.Raghuram, B.B.Krishna, K.P.Rao, P.Venugopal, Effect of cryo-rolling and annealing on microstructure and properties of commercially pure aluminium, *Materials Science and Engineering: A*, 398 (2005) 246-251. <https://doi.org/10.1016/j.msea.2005.03.026>.
- [15] Y.Estrin, A.Vinogradov, Extreme grain refinement by severe plastic deformation: A wealth of challenging science, *Acta Materialia*, 61 (2013) 782-817. <https://doi.org/10.1016/j.actamat.2012.10.038>.
- [16] H. Miyamoto, Corrosion of ultrafine grained materials by severe plastic deformation, an overview, *Materials Transactions*, 57(5) (2016) 559-572. <https://doi.org/10.2320/matertrans.M2015452>.
- [17] G. Shit, S. Ningshen, The effect of severe plastic deformation on the corrosion resistance of AISI type 304L stainless steel, *Journal of Materials Engineering and Performance*, 29(9) (2020) 5696-5709. <http://dx.doi.org/10.1016/j.mtcomm.2020.101429>.
- [18] G. Singh, K.N. Pandey, Effect of cryogenic treatment on properties of materials: A review. *Proceedings of the Institution of Mechanical Engineers, Part E: Journal of Process Mechanical Engineering*, 236(4) (2022) 1758-1773. <https://doi.org/10.1177/09544089221090189>.
- [19] A. Di Schino, J.M. Kenny, Effects of the grain size on the corrosion behavior of refined AISI 304 austenitic stainless steels, *Journal of Materials Science Letters*, 21(20) (2002) 1631-1634. <https://doi.org/10.1023/A:1020338103964>.
- [20] V. Kurup, C.W. Siyasiya, R.J. Mostert, J.Wicks, The influence of full and partial austenitization temperatures on the quench and partition heat treatment process for an advanced high strength steel, In *IOP Conference Series: Materials Science and Engineering*, 430 (1) (2018) 012045. <http://dx.doi.org/10.1088/1757-899X/430/1/012045>.
- [21] P.Movahed, S.Kolahgar, S.P.H. Marashi, M.Porauvari, N. Parvin, The effect of intercritical heat treatment temperature on the tensile properties and work hardening behavior of ferrite-martensite dual phase steel sheets, *Materials Science and Engineering A*, 518 (2009) 1-6. <https://doi.org/10.1016/j.msea.2009.05.046>.
- [22] M. Nadagouda, C. White, D. Lytle, Lead pipe scale analysis using broad-beam argon ion milling to elucidate drinking water corrosion, *Microscopy and Microanalysis*, 17(2) (2011), 284-291. doi:10.1017/S1431927610094353.
- [23] N.M.Anas, T.E.Abiyoye, A.S.Anasyida, B.K.Dhindaw, H.Zuhailawati, I. Azzura, Microstructure, mechanical and corrosion properties of cryorolled-AA5052 at various solution treatment temperatures, *Materials Research Express*, 7 (2020) 016535. <https://doi.org/10.1088/2053-1591/ab636c>.
- [24] J.G. Rosado-Carrasco, W.F. González-Zapatero, C.J. García, C.M. Gómora, D. Jaramillo, R.R. Ambriz, Analysis of the low cycle fatigue behavior of DP980 steel gas metal arc welded joints, *Metals*, 12(3) (2020) 419. <https://doi.org/10.3390/met12030419>.
- [25] R. Verma, A. Srinivasan, R. Jayaganthan, S.K. Nath, S. Goel, Studies on tensile behaviour and microstructural evolution of UFG Mg-4Zn-4Gd alloy processed through hot rolling, *Materials Science and Engineering: A*, 704 (2022) 412-426. <https://doi.org/10.1016/j.msea.2017.08.032>.
- [26] C. Dudu, R.G. Ripeanu, A.C. Drumeanu, A. Dinita, A.M. Lospa, A.M. Evaluation of the corrosion wear speed of different equipment in the water injection treatment plant, *IOP Conference Series: Materials Science and Engineering*, 514, (1) (2019) 012008. <http://dx.doi.org/10.1088/1757-899X/514/1/012008>.
- [27] E. Ahmad, F.Karim, K.Saeed, Manzoor, Tanvir, G.H.Zahid, Effect of cold rolling and annealing on the grain refinement, *Materials Science and Engineering A*, 60 (2014) 1-8. <https://doi.org/10.1088/1757-899X/60/1/012029>.
- [28] D.Singh, P.Nageswara Rao, R.Jayaganthan, Microstructures and impact toughness behavior of Al 5083 alloy processed by cryorolling and afterwards annealing, *International Journal of Minerals, Metallurgy and Materials*, 20 (2013) 759-769. <https://doi.org/10.1007/s12613-013-0794-4>.
- [29] T.Ungar, Microstructural parameters from X-ray diffraction peak broadening, *Scripta Materialia*, 51 (2004) 777-781. <https://doi.org/10.1016/j.scriptamat.2004.05.007>.
- [30] K.S.V.B.R. Krishna, K.S.Chandra, R.Tejas, N.K.Naga, K.Sivaprasad, R.Narayananasamy, K.Venkateswarlu, Effect of cryorolling on the mechanical properties of



- AA5083 alloy and the Portevin-Le Chatelier phenomenon, *Materials and Design*, 67 (2015) 107-117. <https://doi.org/10.1016/j.matdes.2014.11.022>.
- [31] B.Roy, K.Rajesh, D.Jayanta, Effect of cryorolling on the microstructure and tensile properties of bulk nano-austenitic stainless steel, *Materials Science and Engineering A*, 631 (2015) 241-247. <https://doi.org/10.1016/j.msea.2015.02.050>.
- [32] N.Saeidi, F.Ashrafizadeh, B.Niroumand, M.R.Forouzan, F. Barlat, Eng. Damage mechanism and modeling of void nucleation process in a ferrite-martensite dual phase steel, *Engineering Fracture Mechanism*, 127 (2014) 97-103. <https://doi.org/10.1016/j.engfracmech.2014.05.017>.
- [33] M.Soleimani, H.Mirzadeh, C.Dehghanian, Effect of grain size on the corrosion resistance of low carbon steel, *Materials Research Express*, 7(1) (2020) 016522. <https://doi.org/10.1088/2053-1591/ab62fa>.
- [34] S.M.Hasan, A.Haldar, D.Chakrabarti, Microstructure and mechanical properties of cold rolled low carbon steel after prolonged annealing treatment, *Materials Science and Engineering A*, 28 (2012) 823-828. <https://doi.org/10.1179/1743284711Y.0000000113>.

KARAKTERIZACIJA KRIOGENO VALJANOG ČELIKA SA NISKIM UDELOM UGLJENIKA KORISTEĆI POČETNU FERIT-MARTENZIT MIKROSTRUKTURU

S.A.Zakaria ^a, M. S. Ahmad ^a, A.S.Anasyida ^{a,*}, H.Zuhailawati ^a, B.K. Dhindaw ^b, T.E.Abioye ^c

^a Fakultet za inženjering materijala i mineralnih resursa, Univerzitet Sains u Malaziji, Penang, Malazija

^b Indijski institut za tehnologiju, Haragpur, Indija

^c Departman za industrijsko inženjerstvo i proizvodnju, Fakultet za inženjerstvo i tehnologiju, Federalni univerzitet za tehnologiju u Akureu, Akure, Ondo, Nigerija

Apstrakt

Kriovaljanje, tehnika intenzivne plastične deformacije (IPD) izvođena pri kriogenim temperaturama, pokazala se kao obećavajuća tehnika za poboljšanje mikrostrukture i mehaničkih svojstava čelika sa niskim udelom ugljenika. Čelik sa niskim udelom ugljenika sa početnom dvofaznom ferit-martenzit mikrostrukturom podvrgnut je kriogenom valjanju na temperaturi tečnog azota radi proizvodnje limova s različitim stepenima deformacije: 50%, 70% i 90%. Istraživane su mikrostruktura, mehanička svojstva i otpornost na koroziju. Rezultati pokazuju da kriovaljanje efikasno poboljšava mikrostrukturu i dovodi do veće gustine dislokacija i manje veličine zrna kako se stepen deformacije povećava. Uzorak deformisan kriovaljanjem pod 90% ima najveći odnos veličine zrna (35.5), najmanju veličinu kristalita (13.70 nm), najvišu mrežnu deformaciju (74.6×10^{-3}) i najveću gustinu dislokacija u poređenju s uzorcima deformisanim pod 50% i 70%. Ova usavršena mikrostruktura značajno poboljšava mehanička svojstva, pri čemu uzorak deformisan kriovaljanjem pod 90% pokazuje najveću tvrdoću (152 HV), čvrstoću na istezanje (1020 MPa) i čvrstoću pri kidanju (950 MPa), što odgovara povećanju od 175.6%, 344.0% i 466.5%. Osim toga, kriovaljanje pod 90% pokazalo je smanjenje otpornosti na koroziju, s najnižom stopom korozije zabeleženom pri deformaciji od 90% (5.97 mm/god).

Ključne reči: Čelik sa niskim udelom ugljenika; Dvofazna struktura; Ferit-martenzit; Kriogeno valjanje; Mehanička svojstva; Otpornost na koroziju

